Amino Acids (2013) 44:1337–1345
DOI 10.1007/s00726-013-1469-1

ORIGINAL ARTICLE

^{99m}Tc-labeled monomeric and dimeric NGR peptides for SPECT imaging of CD13 receptor in tumor-bearing mice

Wenhui Ma · Fei Kang · Zhe Wang · Weidong Yang · Guiyu Li · Xiaowei Ma · Guoquan Li · Kai Chen · Yingqi Zhang · Jing Wang

Received: 31 October 2012 / Accepted: 11 February 2013 / Published online: 1 March 2013

Abstract CD13 receptor plays a critical role in tumor angiogenesis and metastasis. We therefore aimed to develop ^{99m}Tc-labeled monomeric and dimeric NGR-containing peptides, namely, NGR1 and NGR2, for SPECT imaging of CD13 expression in HepG2 hepatoma xenografts. Both NGR-containing monomer and dimer were synthesized and labeled with ^{99m}Tc. In vivo receptor specificity was demonstrated by successful blocking of tumor uptake of ^{99m}Tc-NGR dimer in the presence of 20 mg/kg NGR2 peptide. Western blot and immunofluorescence staining confirmed the CD13 expression in HepG2 cells. The NGR dimer showed higher binding affinity and cell uptake in vitro than the NGR-containing monomer, presumably due to a multivalency effect. ^{99m}Tc-Labeled monomeric and dimeric NGR-containing peptides were subjected to SPECT imaging and biodistribution studies. SPECT scans were performed in HepG2 tumor-bearing mice at 1, 4, 12, and 24 h post-injection of ~7.4 MBq tracers. The metabolism of tracers was determined in major organs at different time points after injection which demonstrated rapid, significant tumor uptake and slow tumor washout for both traces. Predominant clearance from renal and hepatic system was also observed in ^{99m}Tc-NGR1 and ^{99m}Tc-NGR2. In conclusion, monomeric and dimeric NGR peptide were developed and labeled with ^{99m}Tc successfully, while the high integrin avidity and long retention in tumor make ^{99m}Tc-NGR dimer a promising agent for tumor angiogenesis imaging.

Keywords ^{99m}Tc · NGR · CD13 · Angiogenesis · SPECT

Wenhui Ma and Fei Kang contributed equally to this work.

W. Ma · F. Kang · Z. Wang · W. Yang · G. Li · X. Ma · G. Li
Department of Nuclear Medicine, Xijing Hospital,
Fourth Military Medical University, Xi'an,
Shaanxi 710032, People's Republic of China

K. Chen
Department of Radiology, Molecular Imaging Center,
Keck School of Medicine, University of Southern California,
Los Angeles, CA 90033, USA

Y. Zhang
State Key Laboratory of Cancer Biology, Department
of Pharmacy, Biotechnology Center, The Fourth Military
Medical University, Xi'an, Shaanxi 710032,
People's Republic of China

J. Wang (✉)
Department of Nuclear Medicine, Xijing Hospital,
Fourth Military Medical University, 127# West Changle Road,
Xi'an, Shaanxi 710032, China
e-mail: wangjing@fmmu.edu.cn

Introduction

The metalloexopeptidase CD13/aminopeptidase N (APN) plays a critical role in cancer angiogenesis, invasion and metastasis. The expression of CD13 is up-regulated in endothelial cells within murine and human tumors. Moreover, tissues that undergo angiogenesis blood vessels also overexpress APN (Pasqualini et al. 2000; Bhagwat et al. 2001; Zhang et al. 2005; Petrovic et al. 2007). The asparagine-glycine-arginine (NGR) motif in both cyclic and linear form has previously been shown to specifically bind to aminopeptidase N that is selectively overexpressed on tumor vasculature and some tumor cells (Bhagwat et al. 2001; Negussie et al. 2010).

A series of peptides have been successfully developed with excellent tumor targeted efficacy and favorable in vivo pharmacokinetics (Arap et al. 1998; Curnis et al. 2002; Yang et al. 2006; Meng et al. 2007; Dijkgraaf et al.

2011), such as tTF-NGR, which had the potential of specific delivery of the NGR-containing conjugates to CD13 positive cells (van Hensbergen et al. 2004; Yokoyama and Ramakrishnan 2005; von Wallbrunn et al. 2008; Ndinguri et al. 2009; Zhao et al. 2011). Application of cyclic NGR-labeled paramagnetic quantum dots (cNGR-pQDs) showed cNGR co-localizes with CD13 on neovessels of in magnetic resonance imaging (MRI), while unlabeled pQDs were not only minimally detected with both MRI and two-photon laser scanning microscope (TPLSM) (Oostendorp et al. 2008). Moreover, NGR-hTNF conjugate in combination with standard chemotherapy demonstrated favorable tolerability and preliminary evidence of disease control in pretreated patients (Corti et al. 2010; Gregorc et al. 2010; Santoro et al. 2010; Schwoppe et al. 2010; van Laarhoven et al. 2010).

In this study, monomeric and dimeric NGR peptides were synthesized and labeled with ^{99m}Tc, then subjected to SPECT imaging of CD13 expression in a subcutaneous mouse HepG2 hepatoma xenograft model, which showed positive CD13 receptor and easy formation of tumor.

Materials and methods

General

All chemicals (reagent grade) were obtained from commercial suppliers and used without further purification. NGR1 (GNGRG) and NGR2 [(GNGRG)$_2$KGK] were prepared by SPPS using the Fmoc method on a Chlorotrityl chloride resin. $^{99m}TcO_4^-$ was produced from ^{99}Mo/^{99m}Tc generator (Beijing Atom High Tech, China). Water was purified using a Milli-Q ultra-pure water system from Millipore (Milford, USA), followed by passing through a Chelex 100 resin before bioconjugation and radiolabeling. Radio-TLC was performed on silica gel-coated plastic sheets (Polygram SIL G, Macherey–Nagel) with acetone and Vethanol:Vwater:Vammonia water = 2:5:1 as the eluents. The plates were read with Bioscan Mini-scan (USA) and Allchhrom Plus software. The semi preparative high-performance liquid chromatography (HPLC, Aglint, Canada) was employed for peptide analysis. Mass spectra were obtained on a Q-Tof premier-UPLC system equipped with an electrospray interface (ESI; Waters, USA) or a Thermo Electron Finnigan LTQ mass spectrometer equipped with an electrospray ionization source (Thermo Scientific, USA).

Radiolabeling and formulation

NGR-containing peptides, including the monomeric GNGRG (NGR1), dimeric [(GNGRG)$_2$KGK] (NGR2), and cyclic GCNGRC, were prepared by solid phase peptide synthesis (SPPS) using the Fmoc strategy on chlorotrityl chloride resins as previously reported (Lily Adar et al. 2011). Mass spectra were used to confirm the identity of the products. The fresh $^{99m}TcO_4^-$ solution (37–74 MBq) was added into a solution of NGR peptides (15–20 µg peptide per mCi $^{99m}TcO_4^-$) with 200 µg stannous chloride dissolved in 1 M HCl (5 µg/µL) and 20 µL of 0.2 M NaAc/HAc buffer (pH 4.2) solution. The mixture was incubated at room temperature for 30 min. The $^{99m}TcO_4^-$-containing solutions were filtered over a 0.2 µm syringe filter (Acrodisc, PALL, USA) before being purified by HPLC and then passed through a 0.2 µm Millipore filter into a sterile vial for use.

In vitro stability

The stability of ^{99m}Tc-labeled NGR peptides in PBS (phosphate buffered solution, pH 7.4) and fresh mouse serum was studied at different time points and the percentage of parent tracer was determined by radio-TLC.

Cell culture and animal model

HepG2 cells and HT-29 cells were grown in high glucose DMEM culture medium. All cell lines were cultured in medium supplemented with 10 % (v/v) fetal bovine serum (Gibco, USA), 1 % mycillin and 1 % glutaminate (Beyotime, China) at 37 °C in a humidified atmosphere with 5 % CO_2. Using female BALB/c nude mice (4–6 weeks of age), HepG2 tumor model was established by subcutaneous injection of 2 × 10^6 HepG2 tumor cells (0.1 mL) into the right upper flanks. When the tumor volume reached 0.8–1.0 cm in diameter (2–3 weeks after inoculation), the tumor-bearing mice were used for SPECT imaging and biodistribution studies. All animal studies were approved by Clinical Center at the FMMU.

Western blot analysis of CD13 expression on HepG2 cells

HepG2 and HT-29 cells grown in 75 cm^2 culture flasks were resuspended in lysis buffer (Beyotime, China) supplemented with complete, mini protease inhibitors (Roche, Canada). The cell debris was removed by centrifugation (10,000 rpm at 4 °C for 10 min) and the protein concentration was determined with the Bradford Protein Assay Kit (Beyotime, China). Samples of cell extracts containing 40 µg of protein were loaded on SDS–PAGE gels and transferred to polyvinylidene fluoride membrane filters (Invitrogen, USA). CD13 protein was detected with anti-CD13 antibody (1:100, Santa Cruz, USA) and peroxidase-conjugated secondary antibody (1:400, Invitrogen, USA).

The antigen–antibody complexes on the membranes were visualized with ECL Western Blotting Detection System (Thermo, USA) with ChemiDOC XRS + (Biorad, USA). Actin was also detected with anti-β-actin as an internal control and used for normalization purposes in the densitometric analysis.

Immunofluorescence staining of CD13 expression on HepG2 cells

To examine cellular surface expression of CD13, HepG2 and HT-29 cells were plated into 24-well plates at a density of 5×10^4 cells/well. After overnight incubation, cells were fixed in 4 % paraformaldehye for 10 min. Cells were then washed with PBS (1 N Phosphate Buffered Saline), blocked in normal goat serum (1 %) and then incubated with an anti-CD13 polyclonal antibody H300 (1:100, Santa Cruz, USA) for overnight at 4 °C. Fluorescein isocyanate goat anti-rabbit IgG (1:400, Invitrogen, USA) were used as the secondary antibody. Staining images were acquired with an Olympus IX71 microscope (Japan). DAPI (4, 6-diamidino-2-phenylindole) was used for nucleus staining.

Cell uptake study

HepG2 cells were seeded into 48-well plates at a density of 2×10^5 cells per well, 24 h prior to the experiment. HepG2 cells were then incubated with ^{99m}Tc-labeled NGR peptides (~370 kBq/well) at 37 °C for 15, 30, 60, and 120 min. After incubation, tumor cells were washed three times with ice cold PBS and harvested by trypsinization with 0.25 % trypsin/0.02 % EDTA (Hyclone, USA). Cell suspensions were collected and measured in a gamma counter (Zhida, Shannxi, China). Cell uptake data was presented as percentage of total input radioactivity added to the culture medium after decay correction. Experiments were performed twice with triplicate wells.

Cell-binding assay

In vitro CD13 receptor binding affinity and specificity of ^{99m}Tc-NGR1 and ^{99m}Tc-NGR2 were assessed via competitive cell-binding assay. The best-fit 50 % inhibitory concentration (IC_{50}) values for the HepG2 cells were calculated by fitting the data with non-linear regression using Graph-Pad Prism 5.0 (Graph-Pad Software, San Diego, CA, USA).

SPECT imaging and blocking experiment

HepG2 tumor-bearing animals were imaged in supine position with a one-head SPECT MPR (GE, USA) equipped with a pinhole collimator. About 7.4 MBq of ^{99m}Tc-labeled NGR peptides were intravenously injected into each mouse under intraperitoneal injection of sodium pentobarbital at a dose of 45.0 mg/kg. Static SPECT images were acquired at 1, 4, 12, and 24 h pi. For the blocking experiment, each HepG2 tumor-bearing mouse was scanned after the co-injection of 7.4 MBq of ^{99m}Tc-labeled NGR peptides with 20 mg/kg NGR2. The acquisition count limit was set at 200 k.

Biodistribution studies

HepG2 tumor-bearing mice were injected with ~7.4 MBq of ^{99m}Tc-labeled NGR peptides with or without excess unlabeled NGR peptides (20 mg/kg). At 4 h after injection of the tracer, mice were sacrificed and dissected. The radioactivity in the HepG2 tumor, major organs and muscles were collected and weighed wet with tubes (%ID/g). Mean uptake (%ID/g) for a group of animals was calculated with standard deviations. Values were expressed as mean ± SD ($n = 3$/group).

Statistical analysis

Quantitative data were expressed as mean ± SD. Means were compared using one-way ANOVA and student's t test. P values <0.05 were considered statistically significant.

Results

Chemistry and radiochemistry

Both the monomeric NGR1 and dimeric NGR2 peptides were prepared (Fig. 1). The analytical HPLC and mass spectroscopy were used to confirm the identity of the products. The mass spectroscopy data and chemical structures for NGR1 and NGR2 were represented below (Fig. 1). The electrospray ionization mass spectra of NGR1 and NGR2 were determined to be $m/z = 459.143$ ($[M + H]^+$) and $m/z = 1{,}213.696$ ($[M + H]^+$), respectively. After purification, the specific activity of ^{99m}Tc-labeled tracers was determined to be about 11–16 MBq/nmol for ^{99m}Tc-NGR1 and 22–36 MBq/nmol for ^{99m}Tc-NGR2, respectively. The radiochemical purities of both tracers were >97 %. The in vitro stability of ^{99m}Tc-labeled NGR peptides in PBS (pH 7.4) and fresh mouse serum at 37 °C was shown in Fig. 2. After 12 h of incubation, more than 92 % of ^{99m}Tc-NGR peptides remained intact in PBS as well as mouse serum.

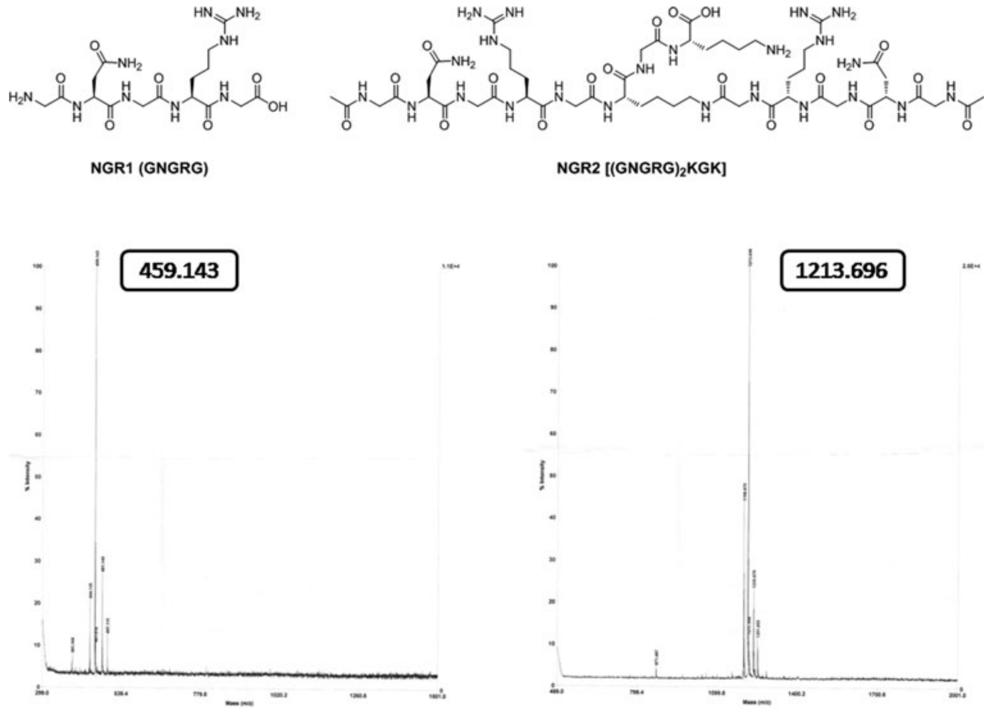

Fig. 1 Chemical structures and mass results of NGR1 (GNGRC) and NGR2 [(GNGRG)2KGK]

Western blotting and immunofluorescence staining

Western blotting analysis of CD13 expression on HepG2 cells showed a positive band that was correlated to the molecular size of CD13, whereas negative band was observed on HT-29 cells (Fig. 3). Visual assessment of fluorescent microscopy analysis indicated that CD13 was overexpressed on the cell surface of HepG2 cells, but not in the case of HT-29 cells, which was consistent with the results from western blotting analysis.

Cell uptake

Cell uptake study revealed that ^{99m}Tc-NGR1 and ^{99m}Tc-NGR2 could bind with HepG2 tumor cells. During the first 15 min, about 0.40 ± 0.02 % of ^{99m}Tc-NGR1 and 0.41 ± 0.19 % of ^{99m}Tc-NGR2 uptake in HepG2 cells were determined. After 2-h incubation, the peptide uptake in HepG2 cells reached the maximum of 1.49 ± 0.11 and 1.74 ± 0.07 %, respectively (Fig. 4a). The amount of ^{99m}Tc-NGR2 uptake in HepG2 cells was higher than that of ^{99m}Tc-NGR1. Both ^{99m}Tc-labeled peptides showed good cell retention. About 1.37 ± 0.18 % of ^{99m}Tc-NGR1 and 1.73 ± 0.12 % of ^{99m}Tc-NGR2 were still associated with HepG2 cells after 4-h incubation.

Cell-binding assay

Ligand-receptor binding affinities of ^{99m}Tc-NGR1 and ^{99m}Tc-NGR2 to CD13 were determined by a competitive

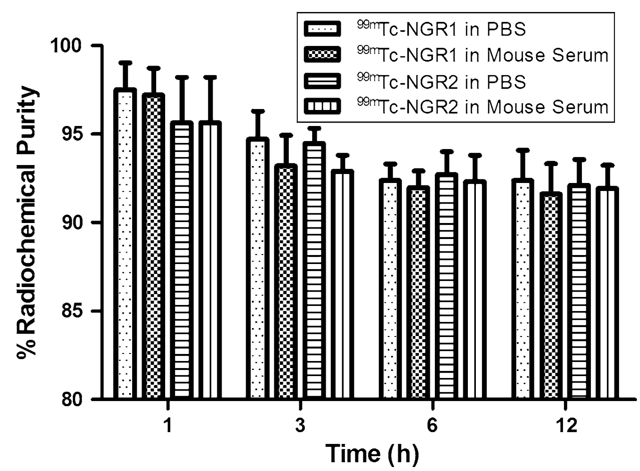

Fig. 2 In vitro stability of ^{99m}Tc-NGR1 and ^{99m}Tc-NGR2 peptides in PBS (pH 7.4) and mouse serum at 37 °C for 1, 3, 6, and 12 h. Their radiochemical purities were >97 %. More than 92 % of ^{99m}Tc-NGR peptides remained intact in PBS and mouse serum after 12 h of incubation

cell-binding assay. Both ^{99m}Tc-labeled peptides inhibited the binding of NGR peptides to HepG2 cells in a concentration-dependent manner (Fig. 4b). The IC_{50} values for ^{99m}Tc-NGR1 and ^{99m}Tc-NGR2 were calculated to be 223 ± 23 and 157 ± 15 nmol/L, respectively.

SPECT imaging

The tumor-targeting efficacy of ^{99m}Tc-NGR probes in HepG2 tumor-bearing nude mice was evaluated by static

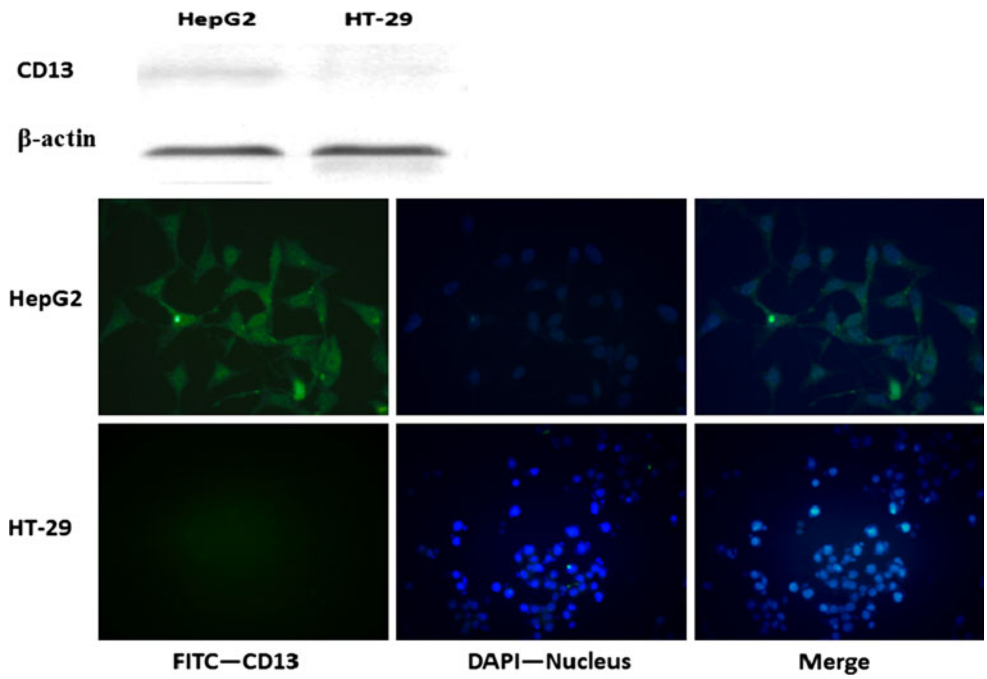

Fig. 3 Western blot and immunofluorescence staining showed that CD13 expression of HepG2 was positive and HT-29 cell was negative(×40, representative images of CD13 expression with *green* FITC and nucleus with *blue* DAPI) (color figure online)

SPECT scans at different time points after injection. Representative decay-corrected images were shown in Fig. 5. The HepG2 tumors were clearly visualized with good tumor-to-background contrast for both tracers. Significant tumor uptake reductions were observed in a blocking study. Co-injection of ^{99m}Tc-NGR2 with a blocking dose of NGR2, ^{99m}Tc-NGR2 was cleared from the body significantly faster and the uptake in most of the organs was lower than those without blocking agent. Overall, ^{99m}Tc-NGR2 provided better image quality with the same amount of injected activity.

Biodistribution studies

Tissue distribution data for ^{99m}Tc-NGR1 and ^{99m}Tc-NGR2 in mice bearing HepG2 hepatoma tumors were given as percentage administered activity per gram of tissue (%ID/g) in Table 1 and Fig. 6. In vivo biodistribution of with and without co-injection of non-radiolabeled NGR2 peptide (20 mg/kg of mouse body weight) was examined in HepG2 tumor-bearing mice. For ^{99m}Tc-NGR1, the tumor uptake was determined to be 3.47 ± 1.52, 2.67 ± 0.68, 1.90 ± 0.47 and 1.50 ± 0.67 %ID/g at 1, 4, 12, and 24 h, respectively. For ^{99m}Tc-NGR2, the tumor uptake was 6.22 ± 1.23, 5.03 ± 0.74, 3.74 ± 0.78 and 2.28 ± 1.29 %ID/g at 1, 4, 12, and 24 h, respectively (Fig. 6a, b). Both tracers were excreted mainly through the kidneys. ^{99m}Tc-NGR1 exhibited 15.87 ± 1.76 %ID/g kidney uptake compared with 17.76 ± 2.87 %ID/g in ^{99m}Tc-NGR2 at 1 h pi ($P > 0.05$). ^{99m}Tc-NGR2 showed 15.87 ± 1.76 %ID/g of liver uptake that is higher than that of the monomer (10.30 ± 1.32 %ID/g). This result might be attributed to the relatively large molecular size of NGR dimer. The non-specific uptake in the muscle was at a very low level for both tracers. Both compounds had comparable liver and muscle uptake. ^{99m}Tc-NGR2 exhibited higher tumor uptake at the early time point and better tumor retention (Fig. 6b), indicating the longer circulation time. In addition, ^{99m}Tc-NGR2 showed higher tumor uptake compared to ^{99m}Tc-NGR1, but the tumor-to-kidney ratio of ^{99m}Tc-NGR2 was significantly lower than ^{99m}Tc-NGR1. Similar tumor/muscle, tumor/liver, tumor/kidney, and tumor/heart ratios were observed for ^{99m}Tc-NGR1 and ^{99m}Tc-NGR2, while the absolute tumor uptake of ^{99m}Tc-NGR2 was significantly higher than that of ^{99m}Tc-NGR1 ($P < 0.01$).

A decrease of radioactivity was observed in all dissected tissues and organs, which was similar to SPECT imaging results in blocking group (Fig. 7), with the change of tumor uptake being the most significant reducing markedly from 5.03 ± 0.74 %ID/g, whereas the presence of non-labeled NGR peptides significantly reduced to 2.65 ± 0.21 %ID/g at 4 h after injection. For ^{99m}Tc-NGR2 non-blocking group, 10.93 ± 1.98 %ID/g in liver and 9.06 ± 0.67 %ID/g in kidney were decreased to 8.17 ± 0.16 and 6.93 ± 0.97 %ID/g by blocking, respectively.

Discussion

The development of radiolabeled peptides for diagnostic and therapeutic applications has expanded exponentially in the

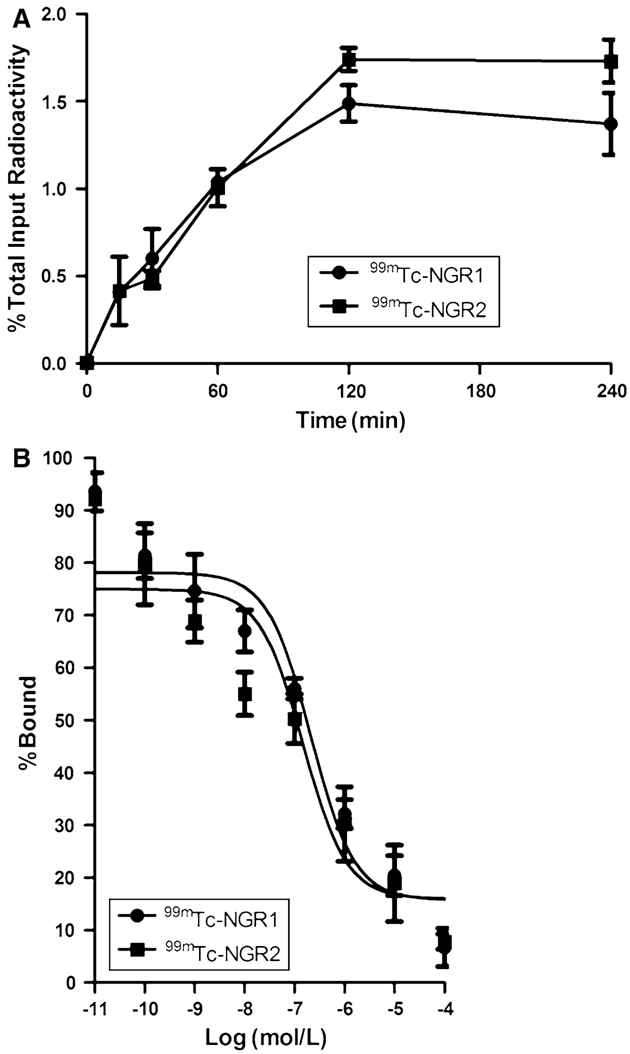

Fig. 4 Cell uptake and cell-binding studies using HepG2 human hepatoma cells. **a** Cell uptake of ^{99m}Tc-labeled NGR monomer and dimer ($n = 3$, mean ± SD). The background readings are reflected at time 0. About 1.37 ± 0.18 % of ^{99m}Tc-NGR1 and 1.73 ± 0.12 % of ^{99m}Tc-NGR2 were still associated with HepG2 cells after 4-h incubation. **b** Cell binding of ^{99m}Tc-NGR1 and ^{99m}Tc-NGR2 to the CD13 receptors overexpressed on HepG2 cells ($n = 3$, mean ± SD)

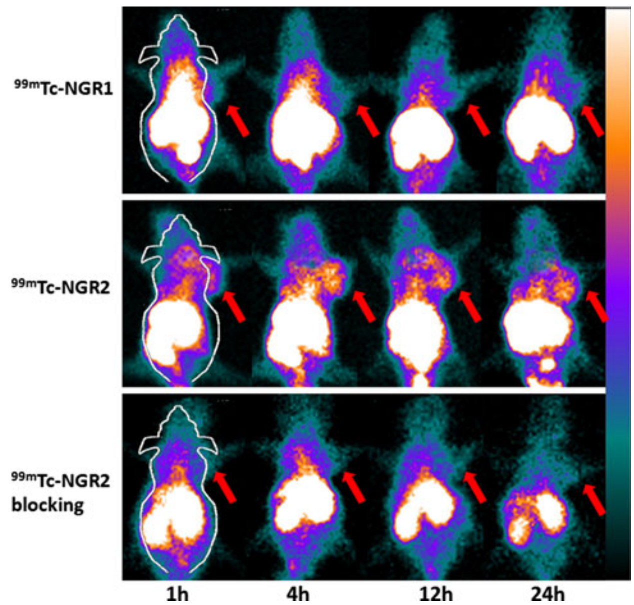

Fig. 5 Representative decay-corrected whole-body SPECT images of mice bearing HepG2 tumors on right front flank after intravenous administration ~7.4 MBq of ^{99m}Tc-NGR1 and ^{99m}Tc-NGR2, with and without co-injection of 20 mg/kg of NGR2 peptides as a blocking agent at 1, 4, 12, and 24 h pi. Tumors were indicated by *red arrows*

last decades (Wu et al. 2005; Dijkgraaf et al. 2011; Chen et al. 2012). Peptide-based radiopharmaceuticals can be produced easily and inexpensively, and have many favorable properties, including fast clearance, rapid tissue penetration, and low antigenicity (Arap et al. 1998; Meng et al. 2007; Ndinguri et al. 2009; Chen and Conti 2010; Corti et al. 2010). CD13 receptor is an attractive biological target, which has been found to be overexpressed on newly formed neovasculature and on a wide range of tumor cells types. In this study, we developed ^{99m}Tc-labeled NGR peptides for HepG2 tumor imaging. To our knowledge, this is the first SPECT imaging study to evaluate ^{99m}Tc-labeled NGR peptides (monomer and dimer) in a HepG2 tumor mouse model.

We constructed monomeric and dimeric NGR peptides and labeled with ^{99m}Tc in moderate yields (>92 % for both peptides). Both ^{99m}Tc-labeled tracers showed good stability in PBS and mouse serum. Western blot and immunofluorescence staining confirmed that CD13 receptor was overexpressed on HepG2 cells. The cell binding showed that NGR dimer had a higher affinity than monomer (Fig. 3), presumably due to a multivalency effect. The term multivalency effect described the use of more than one targeting ligand in a single reagent for simultaneously binding to multiple receptors to enhance the overall binding affinity. Others had reported that polymeric RGD peptide with more repeating cyclic RGD units significantly enhanced the binding affinity of RGD ligand to integrin $\alpha_v\beta_3$ receptor due to multivalency effect (Chen et al. 2004; Wu et al. 2005; Dijkgraaf et al. 2011; Lily Adar et al. 2011).

^{99m}Tc-labeled NGR peptides SPECT scans in a HepG2 hepatoma mouse model showed both ^{99m}Tc-NGR1 and ^{99m}Tc-NGR2 had a notable uptake in the HepG2 tumor, and dominant renal and hepatic clearance. Apparently, ^{99m}Tc-NGR2 had higher tumor uptake than ^{99m}Tc-NGR1 at different time points investigated, while ^{99m}Tc-NGR2 exhibited similar kidney and liver uptake compared with ^{99m}Tc-NGR1 (Fig. 5). Dimer showed higher uptake especially in living animal model than monomer because CD13 receptor was not only overexpressed on endothelial cell of neovessels but also on HepG2 cell, although color bar of

Table 1 Biodistribution data (%ID/g, mean ± SD) of ^{99m}Tc-NGR1 and ^{99m}Tc-NGR2 in HepG2 hematoma tumor-bearing nude mice at 1, 4, 12, and 24 h pi ($n = 5$)

	^{99m}Tc-NGR1				^{99m}Tc-NGR2			
Organs	1 h	4 h	12 h	24 h	1 h	4 h	12 h	24 h
Liver	10.30 ± 1.32	7.85 ± 0.96	4.25 ± 1.25	2.22 ± 0.31	15.67 ± 1.67	9.07 ± 0.67	5.64 ± 1.74	3.13 ± 0.83
Kidney	15.87 ± 1.76	9.06 ± 1.26	5.30 ± 0.30	4.11 ± 0.81	17.76 ± 2.87	10.93 ± 1.98	4.87 ± 0.87	3.04 ± 0.34
Muscle	0.97 ± 0.07	0.89 ± 0.03	0.77 ± 0.14	0.44 ± 0.14	0.86 ± 0.06	0.83 ± 0.04	0.33 ± 0.13	0.24 ± 0.14
Tumor	3.47 ± 1.52	2.67 ± 0.68	1.90 ± 1.50	1.50 ± 0.67	6.22 ± 1.23	5.03 ± 0.74	3.74 ± 0.78	2.28 ± 1.29

Tumor-to-normal tissue ratios at 1-h post-injection	^{99m}Tc-NGR1	^{99m}Tc-NGR2
Tumor/muscle	3.59	6.26
Tumor/kidney	0.22	0.35
Tumor/liver	0.34	0.40

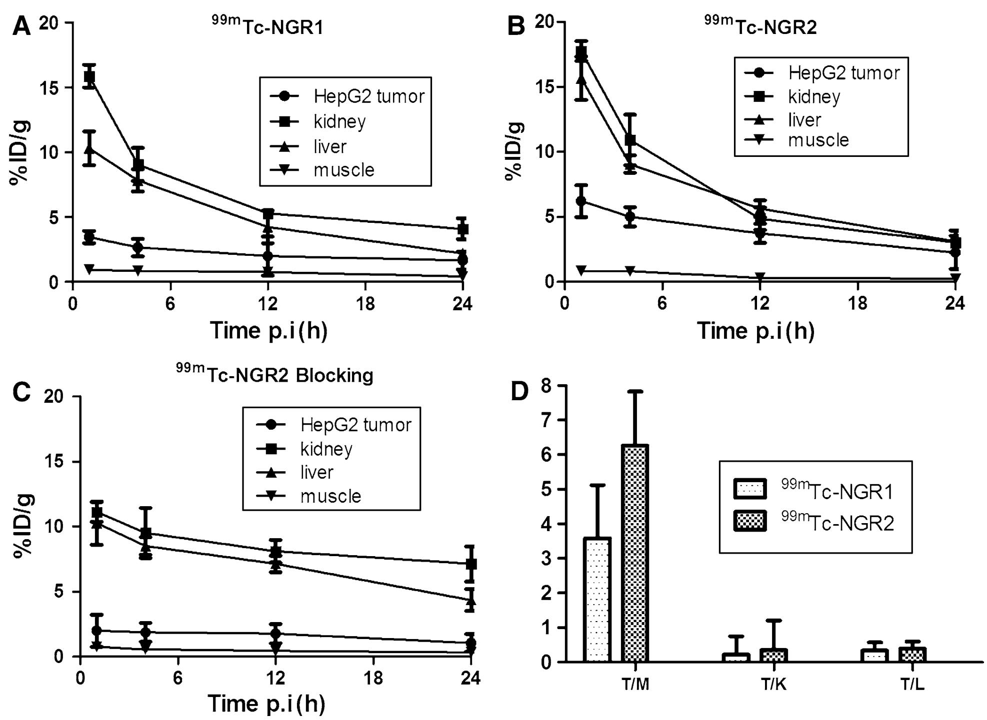

Fig. 6 Biodistribution of ^{99m}Tc-NGR1 (**a**), ^{99m}Tc-NGR2 (**b**), and ^{99m}Tc-NGR2 co-injection with 20 mg/kg NGR2 (**c**) in HepG2 tumor, liver, kidney, and muscle after intravenous injection of ~7.4 MBq of ^{99m}Tc-NGR1 or ^{99m}Tc-NGR2 peptide. Ratio of tumor-to-major organs (muscle, kidney, and liver) based on the biodistribution data at 1-h post-injection. Error bar was calculated as the standard deviation ($n = 5$, mean ± SD)

images was adjusted to comparison. In addition, our study showed that ^{99m}Tc-NGR2 was superior to ^{99m}Tc-NGR1 in terms of both tumor uptake and tumor/background contrast, because ^{99m}Tc-NGR1 with relatively small molecular size led to shorter retention time and worse imaging quality than ^{99m}Tc-NGR2. Interestingly, although ^{99m}Tc-NGR2 demonstrated significantly higher tumor uptake than ^{99m}Tc-NGR1, the tumor/kidney ratio of the dimer was not higher than that of monomer ($P > 0.05$) at the later time point (12 h pi). This could be contributed to the clearance of ^{99m}Tc-NGR2 from the kidney with a large amount. In addition, although ^{99m}Tc-NGR1 and ^{99m}Tc-NGR2 had comparable tumor/kidney and tumor/liver ratios (Fig. 6d), tumor/muscle ratio of ^{99m}Tc-NGR2 was about twofold higher than that of the monomer, providing better imaging quality of ^{99m}Tc-NGR2 over than that of ^{99m}Tc-NGR1. The receptor specificity of ^{99m}Tc-NGR2 was further confirmed by effective inhibition of tumor uptake in the presence of excess non-labeled NGR2 peptide in both SPECT imaging and biodistribution studies (Figs. 5, 6).

In summary, our data demonstrated that ^{99m}Tc-NGR2 is a better SPECT imaging agent than ^{99m}Tc-NGR1 in terms of in vitro and in vivo properties. Our future work will focus on the development of radiolabeled NGR multimer derivatives, as well as determine whether the tumor/background ratio derived from SPECT imaging or biodistribution truly reflects the tumor–receptor expression level. Developing small but specific fusion protein conjugated with NGR peptide is also

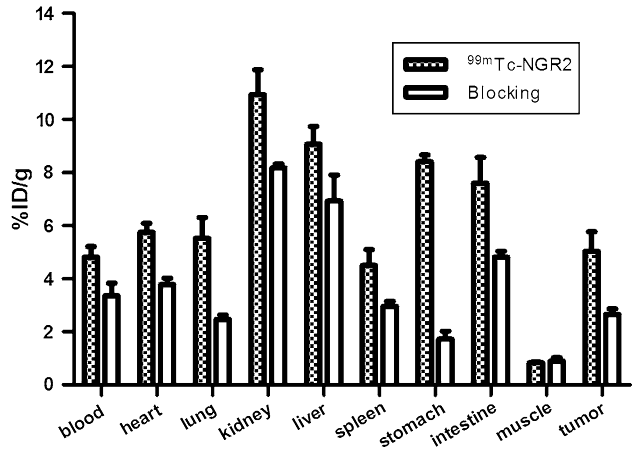

Fig. 7 Biodistribution of ^{99m}Tc-NGR2 in HepG2 tumor-bearing athymic nude mice at 4 h with and without co-injection of 20 mg/kg of NGR2 peptide as a blocking agent (n = 5, mean ± SD)

worthy to explore (Corti and Ponzoni 2004; Kessler et al. 2008; Lei et al. 2010). Because ^{99m}Tc-NGR1 and ^{99m}Tc-NGR2 showed high uptake in liver and kidney for their chemical structure and features of peptides' excretion, optimal approach to reduce liver and kidney uptake is needed to image urological and hepatic malignancies (Ruggiero et al. 2010). In addition, a thorough comparison between radiolabeled NGR peptides and other angiogenesis-targeted probes, such as RGD (Arg-Gly-Asp peptide), is warranted to further determine the advantages of new radiotracers.

Conclusion

Monomeric and dimeric NGR peptides were successfully labeled with the generator-produced ^{99m}Tc for SPECT imaging of tumor CD13 receptor. The dimeric ^{99m}Tc-NGR2 exhibited overall better properties in vitro and in vivo as compared to monomeric ^{99m}Tc-NGR1, in terms of binding affinity, cellular uptake, tumor uptake and retention, and pharmacokinetics. ^{99m}Tc-NGR2 peptide is a promising SPECT agent for imaging of tumor angiogenesis.

Acknowledgments This work was supported by the National Natural Science Foundation of China (Grant No. 30970847, 30800275, 30970846), the Program of the National Basic Research and Development Program of China (Grant No. 2011CB707704), and the Major Program of National Natural Science Foundation of China (Grant No. 81090274).

References

Arap W, Pasqualini R et al (1998) Cancer treatment by targeted drug delivery to tumor vasculature in a mouse model. Science 279(5349):377–380

Bhagwat SV, Lahdenranta J et al (2001) CD13/APN is activated by angiogenic signals and is essential for capillary tube formation. Blood 97(3):652–659

Chen K, Conti PS (2010) Target-specific delivery of peptide-based probes for PET imaging. Adv Drug Deliv Rev 62(11):1005–1022

Chen X, Tohme M et al (2004) Micro-PET imaging of alphavbeta3-integrin expression with 18F-labeled dimeric RGD peptide. Mol Imaging 3(2):96–104

Chen K, Sun X et al (2012) Evaluation of (6)(4)Cu labeled GX1: a phage display peptide probe for PET imaging of tumor vasculature. Mol Imaging Biol 14(1):96–105

Corti A, Ponzoni M (2004) Tumor vascular targeting with tumor necrosis factor alpha and chemotherapeutic drugs. Ann N Y Acad Sci 1028:104–112

Corti A, Giovannini M et al (2010) Immunomodulatory agents with antivascular activity in the treatment of non-small cell lung cancer: focus on TLR9 Agonists, IMiDs and NGR-TNF. J Oncol 2010:732680

Curnis F, Arrigoni G et al (2002) Differential binding of drugs containing the NGR motif to CD13 isoforms in tumor vessels, epithelia, and myeloid cells. Cancer Res 62(3):867–874

Dijkgraaf I, Yim CB et al (2011) PET imaging of alphavbeta(3) integrin expression in tumours with (6)(8)Ga-labelled mono-, di- and tetrameric RGD peptides. Eur J Nucl Med Mol Imaging 38(1):128–137

Gregorc V, Zucali PA et al (2010) Phase II study of asparagine-glycine-arginine-human tumor necrosis factor alpha, a selective vascular targeting agent, in previously treated patients with malignant pleural mesothelioma. J Clin Oncol 28(15):2604–2611

Kessler T, Schwoppe C et al (2008) Generation of fusion proteins for selective occlusion of tumor vessels. Curr Drug Discov Technol 5(1):1–8

Lei H, Cao P et al (2010) Expression and functional characterization of tumor-targeted fusion protein composed of NGR peptide and 15-kDa actin fragment. Appl Biochem Biotechnol 162(4):988–995

Lily Adar YS, Journoa Gal, David Ayelet (2011) Pro-apoptotic peptide-polymer conjugates to induce mitochondrial-dependent cell death. Polym Adv Technol 22:199–208

Meng J, Yan Z et al (2007) High-yield expression, purification and characterization of tumor-targeted IFN-alpha2a. Cytotherapy 9(1):60–68

Ndinguri MW, Solipuram R et al (2009) Peptide targeting of platinum anti-cancer drugs. Bioconjug Chem 20(10):1869–1878

Negussie AH, Miller JL et al (2010) Synthesis and in vitro evaluation of cyclic NGR peptide targeted thermally sensitive liposome. J Control Release 143(2):265–273

Oostendorp M, Douma K et al (2008) Quantitative molecular magnetic resonance imaging of tumor angiogenesis using cNGR-labeled paramagnetic quantum dots. Cancer Res 68(18):7676–7683

Pasqualini R, Koivunen E et al (2000) Aminopeptidase N is a receptor for tumor-homing peptides and a target for inhibiting angiogenesis. Cancer Res 60(3):722–727

Petrovic N, Schacke W et al (2007) CD13/APN regulates endothelial invasion and filopodia formation. Blood 110(1):142–150

Ruggiero A, Brader P et al (2010) Different strategies for reducing intestinal background radioactivity associated with imaging HSV1-tk expression using established radionucleoside probes. Mol Imaging 9(1):47–58

Santoro A, Rimassa L et al (2010) Phase II study of NGR-hTNF, a selective vascular targeting agent, in patients with metastatic colorectal cancer after failure of standard therapy. Eur J Cancer 46(15):2746–2752

Schwoppe C, Kessler T et al (2010) Tissue-factor fusion proteins induce occlusion of tumor vessels. Thromb Res 125(Suppl 2):S143–S150

van Hensbergen Y, Broxterman HJ et al (2004) Reduced growth, increased vascular area, and reduced response to cisplatin in

CD13-overexpressing human ovarian cancer xenografts. Clin Cancer Res 10(3):1180–1191

van Laarhoven HW, Fiedler W et al (2010) Phase I clinical and magnetic resonance imaging study of the vascular agent NGR-hTNF in patients with advanced cancers (European Organization for Research and Treatment of Cancer Study 16041). Clin Cancer Res 16(4):1315–1323

von Wallbrunn A, Waldeck J et al (2008) In vivo optical imaging of CD13/APN-expression in tumor xenografts. J Biomed Opt 13(1):011007

Wu Y, Zhang X et al (2005) Micropet imaging of glioma integrin {alpha}v{beta}3 expression using (64)Cu-labeled tetrameric RGD peptide. J Nucl Med 46(10):1707–1718

Yang YS, Zhang X et al (2006) Comparative in vitro and in vivo evaluation of two 64Cu-labeled bombesin analogs in a mouse model of human prostate adenocarcinoma. Nucl Med Biol 33(3): 371–380

Yokoyama Y, Ramakrishnan S (2005) Addition of an aminopeptidase N-binding sequence to human endostatin improves inhibition of ovarian carcinoma growth. Cancer 104(2):321–331

Zhang Z, Harada H et al (2005) Aminopeptidase N/CD13 targeting fluorescent probes: synthesis and application to tumor cell imaging. Peptides 26(11):2182–2187

Zhao BJ, Ke XY et al (2011) The antiangiogenic efficacy of NGR-modified PEG-DSPE micelles containing paclitaxel (NGR-M-PTX) for the treatment of glioma in rats. J Drug Target 19(5): 382–390